Microstructure investigation of semi-polar (11-22) GaN overgrown on differently designed micro-rod array templates

Y. Zhang, J. Bai, Y. Hou, X. Yu, Y. Gong, R. M. Smith, and T. Wang

---

Articles you may be interested in

Microstructure investigation of semi-polar (11-22) GaN overgrown on differently designed micro-rod array templates

Y. Zhang, J. Bai, Y. Hou, X. Yu, Y. Gong, R. M. Smith, and T. Wang[a)]

Department of Electronic and Electrical Engineering, University of Sheffield, Mappin Street, Sheffield S1 3JD, United Kingdom

In order to realize semi-polar (11-22) GaN based laser diodes grown on sapphire, it is necessary to further improve the crystal quality of the (11-22) GaN obtained by using our overgrowth approach developed on regularly arrayed micro-rod templates [T. Wang, Semicond. Sci. Technol. **31**, 093003 (2016)]. This can be achieved by carefully designing micro-rod templates. Based on transmission electron microscopy and photoluminescence measurements, it has been found that the micro-rod diameter plays a vital role in effectively reducing both the dislocation density and the basal staking fault (BSF) density of the overgrown (11-22) GaN, but in different manners. The BSF density reduces monotonically with increasing the micro-rod diameter from 2 to 5 μm, and then starts to be saturated when the micro-rod diameter further increases. In contrast, the dislocation density reduces significantly when the micro-rod diameter increases from 2 to 4 μm, and then starts to increase when the diameter further increases to 5 μm. Furthermore, employing shorter micro-rods is useful for removing additional BSFs, leading to further improvement in crystal quality. The results presented provide a very promising approach to eventually achieving (11-22) semi-polar III-nitride laser diodes. © 2016 Author(s). All article content, except where otherwise noted, is licensed under a Creative Commons Attribution (CC BY) license (http://creativecommons.org/licenses/by/4.0/). [http://dx.doi.org/10.1063/1.4972403]

Semi-polar GaN, particularly in the (11-22) orientation, has emerged to be a promising candidate for fabricating both light emitting diodes (LEDs) and laser diodes (LDs) with a long wavelength beyond the blue spectral region, e.g., green and yellow, which is critical for solid state lighting, visible light communications and opto-genetics. The current status of the development of (11-22) GaN on sapphire can be referred to a topical review published very recently.[1] In comparison with the (0001) polar orientation, InGaN/GaN based emitters grown along the (11-22) direction are subjected to significantly reduced piezoelectric polarization fields, thus effectively increasing their internal quantum efficiency (IQE) by reducing the associated quantum confined stark effect (QCSE).[2–4] Furthermore, the (11-22) plane has been predicted to exhibit a lower indium chemical potential than either non-polar or polar surfaces,[5] making (11-22) GaN accommodate indium atoms more easily than either non-polar or polar GaN. Consequently, (11-22) GaN becomes particularly important for achieving longer wavelength emission where high indium content is required. However, semi-polar (11-22) GaN on industry-preferred substrates, such as sapphire, usually contains a high density of defects, including threading dislocations, basal stacking faults (BSFs), and associated partial dislocations.[6] These extended defects are expected to affect the optical performance of semi-polar GaN based devices. In order to address these material challenges, our group has developed a cost-effective approach of overgrowth on regularly arrayed micro-rod templates and thus has achieved semi-polar (11-22) GaN on sapphire with significantly improved crystal quality. Based on such overgrown semi-polar (11-22) GaN, we have demonstrated high-performance semi-polar InGaN LEDs with an emission wavelength of up to the amber spectral region.[7]

However, it is still a great challenge to achieve lasing on (11-22) GaN on sapphire. So far, all the semi-polar III-nitride laser structures have been grown exclusively on extremely expensive free-standing semi-polar GaN substrates.[1,8,9] Therefore, it implies that it is necessary to further improve the crystal quality of any overgrown (11-22) GaN on sapphire in order to achieving lasing. In this paper, by carefully designing micro-rod templates used for our overgrowth, in particular, the diameter and height of the micro-rods used (two major parameters), we have achieved (11-22) semi-polar GaN with best crystal quality on sapphire, which has been systematically studied as a function of the micro-rod parameters by means of multiple characterization methods including photoluminescence (PL), transmission electron microscopy (TEM) and X-ray diffraction (XRD). Furthermore, it has been found that the reduction of both the dislocation density and the BSF density of the overgrown (11-22) GaN is significantly affected by the micro-rod parameters, in particular, the micro-rod diameter, but in different manners. These studies have directly led to stimulated emission very recently achieved on our semi-polar (11-22) GaN on sapphire[10] which has never been reported previously.

Two kinds of single layers of (11-22) GaN (one with a thickness of 1.3 μm and another with 0.4 μm), which will be subsequently fabricated into micro-rod array templates, are grown on *m-plane* sapphire using our high temperature AlN buffer approach by metal organic chemical vapour deposition (MOCVD).[11] For the fabrication of the micro-rod

a)Author to whom correspondence should be addressed. Electronic mail: t.wang@sheffield.ac.uk

templates, a 500 nm SiO_2 layer is initially deposited by plasma enhanced chemical vapor deposition (PECVD), followed by a standard photolithography patterning process. Regularly arrayed SiO_2 micro-rods can be achieved by dry etching processes, and the SiO_2 micro-rods then serve as a second mask to etch the GaN underneath in order to form regularly arrayed GaN micro-rods with the SiO_2 remaining on their top. Both the diameter and the spacing of the micro-rods can be accurately controlled, which simply depend on the micro-rod mask used. A set of micro-rod masks, whose diameters are 2, 2.5, 3, 4, 5, and 7 μm, respectively, have been employed for the fabrication of the micro-rod array templates which will be used for subsequent overgrowth. A study based on a wide range of micro-rod diameters used helps to draw a clear conclusion on the influences of the micro-rod diameter on the reduction of both dislocation density and BSF density. This cannot be achieved using the micro-rod templates with a micro-rod diameter of $\leq 3.5\ \mu m$, as reported previously.[12] For details of our overgrowth and micro-rod template fabrication, refer to our papers published previously.[12]

Figure 1(a) shows the low temperature (10 K) photoluminescence (PL) spectra of the semi-polar (11-22) GaN overgrown on the regularly arrayed micro-rods with different diameters ranging from 2 to 7 μm. The samples were held in a helium closed-circuit refrigerator. A 325 nm continuous wave (CW) He-Cd laser was used as an excitation source, and luminescence was dispersed using a 0.5 m monochromator and detected using a thermoelectrically (TE) cooled charge-coupled detector (CCD) which can be cooled down to $-70\,^{\circ}C$. As usual, two emission peaks have been observed in each spectrum, one at 356 nm which is attributed to the near band-edge (NBE) emission, and another at 363 nm which is related to the BSFs.[13,14] The PL intensity ratio of the NBE emission to the BSF-related emission has been plotted as a function of the micro-rod diameter as shown in Figure 1(b), indicating that with increasing the micro-rod diameter, the ratio exhibits a huge increase from 0.4 to 7.8. It indicates a significant reduction in the BSF density of our samples with increasing the micro-rod diameter.

TEM measurements have been performed on these samples using a Philips EM430 TEM operating at 200 kV. TEM specimens were prepared by mechanical polishing, followed by an ion beam milling process for electron transparency. Figure 2(a) presents the bright field plan-view TEM images of the overgrown (11-22) GaN on the micro-rod templates fabricated using different micro-rod diameters of 2, 3, 4, and 5 μm, respectively. It should be mentioned that the height of the micro-rods with a micro-rod diameter of 2 or 3 μm (D = 2 μm and D = 3 μm) is 1.3 μm, while those in the other two (D = 4 μm and D = 5 μm) have a height of 0.4 μm. The specimens are tilted around $32°$ to the [-1-120] zone-axis from the surface normal. From the invisibility criterion, BSFs can be observed when the diffraction vector g is 10-10.[15] Figure 2(a) clearly exhibits a periodic distribution of the BSF clusters and BSF-free areas along the c-projection direction across the surface. The width of the BSF-free area clearly increases with increasing the micro-rod diameter, leading to a reduction in BSF density from $1.4 \times 10^5\ cm^{-1}$
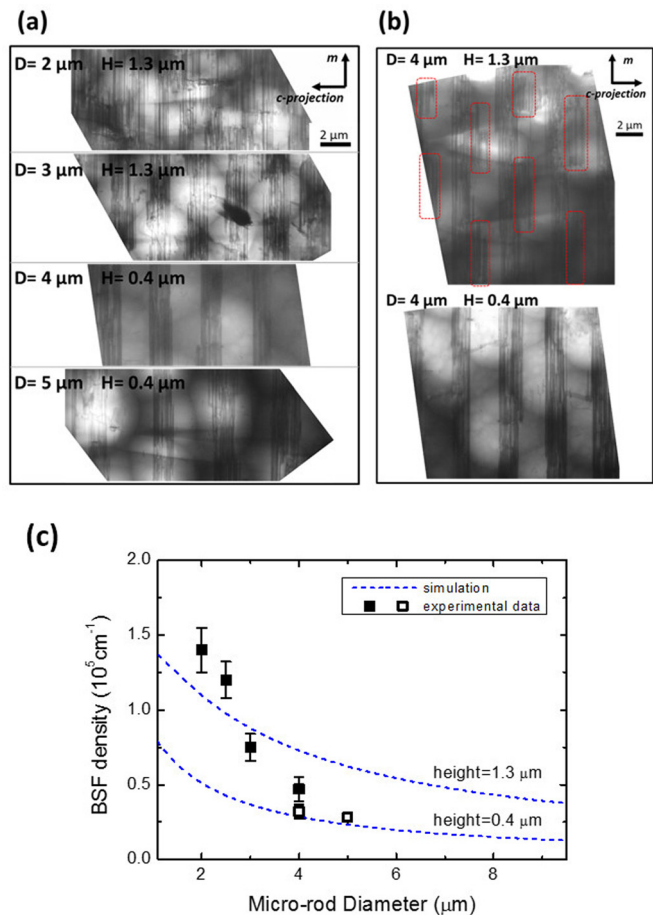
FIG. 2. (a) Bright field plan-view TEM images of the (11–22) GaN overgrown on micro-rods with different diameters and heights (D: diameter, H: height), as labeled in each figure, where the specimens are viewed along the [-1-120] zone-axis with the diffraction vector $g = 10\text{-}10$ to show the BSF distribution across the surface; (b) Bright field plan-view TEM images of the (11-22) GaN overgrown on the micro–rods with a same micro-rod diameter, but different heights of 1.3 and 0.4 μm, respectively; (c) BSF density of the overgrown (11-22) GaN as a function of the micro-rod diameter. Filled and open symbols represent the micro-rods with different heights of 1.3 and 0.4 μm, respectively. The dash lines are the simulation results based on a defection reduction model.
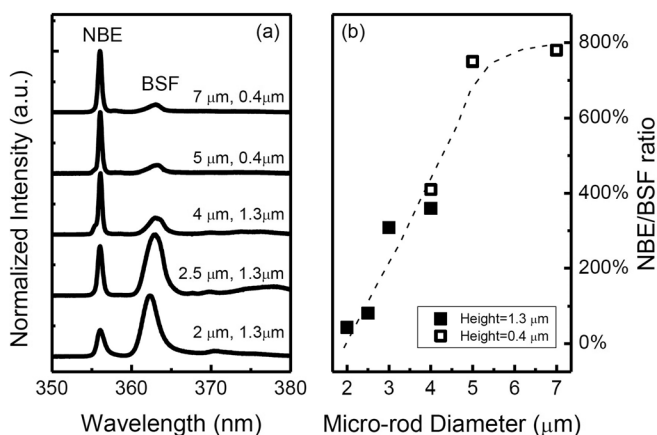

FIG. 1. (a) Low temperature PL spectra of the (11-22) GaN overgrown on micro-rods with different diameters and heights; (b) PL intensity ratio of the NBE emission to the BSF-related emission is plotted as a function of the micro-rod diameter. The dashed line is a guide to the eye.

in the sample of using a 2 μm micro-rod diameter to 2.8 × 10^4 cm^{-1} in the sample of using a 5 μm micro-rod diameter. It has been understood that the BSFs can penetrate from the micro-rod GaN underneath to the surface only when the overgrowth (starting from the sidewalls of micro-rods) is along the *a*-direction, while the growth along the *c*-direction leads to free-BSFs.[12] Furthermore, the growth rate along the *c*-direction is usually higher than that along the *a*-direction. Consequently, the utilization of larger micro-rods along with an increased spacing between micro-rods allows the growth along the *c*-direction to more effectively block the penetration of the BSFs caused due to the growth along the *a*-direction. In addition, the width of the BSF clusters does not change significantly with changing the micro-rod diameter as predicted by our model.[12] Therefore, the utilization of larger micro-rods for overgrowth can significantly reduce the BSF density, although the overgrowth conditions need to be further optimized in order to maintain quick coalescence.

The influence of the micro-rod height on BSF density has also been investigated. Figure 2(b) shows the plane-view TEM images of two semi-polar (11-22) GaN films overgrown on the micro-rod templates fabricated using a same micro-rod diameter (4 μm), but with different micro-rod heights (1.3 and 0.4 μm, respectively). In the case of using micro-rods with the 1.3 μm height, beside the long BSF clusters, additional BSF clusters with a periodic distribution have been observed as marked by red dashed lines. From the surface striation direction (parallel to the [11-2-3]-direction), it can be determined that these additional BSF clusters are distributed along the *c*-projection side. However, in the case of using the 0.4 μm height, the TEM image exhibits a sharp interface between the BSF regions and the defect-free areas, namely, there are no such additional BSF clusters. Generally speaking, employing shorter micro-rods for overgrowth leads to less variation of the diameter of each micro-rod from its bottom to top along the vertical direction. As a result, both the SiO$_2$ on the top of each micro-rod and the growth along the *c*-direction can effectively stop the penetration of the extra BSFs generated due to the variation of the micro-rod diameter. This is consistent with the low temperature PL results showed above. Figure 2(c) shows the BSF density of the overgrown (11-22) GaN samples as a function of the micro-rod diameter. Filled and open symbols represent the micro-rods with a height of 1.3 and 0.4 μm, respectively. The BSF density exhibits a clear reduction on the samples grown on larger and shorter micro-rods, agreeing well with our previous prediction based on a model for defect reduction[12] shown by blue dashed lines in the figure. The simulation was made assuming a BSF density of 4 × 10^5 cm^{-1} in the as-grown GaN template used for the fabrication of micro-rod arrays.

Dislocation distribution is also revealed in the TEM observation by tilting the sample at an angle around 7.5° from the surface normal to view along the [22-43] zone-axis. In Figure 3(a) taken with the diffraction vector *g* = 1-212 (Figure 3(b)), dislocations including *a*-type, *c*-type, mixed type, and Frank-Shockley partial dislocation ($\boldsymbol{b}$ = 1/6 ⟨20-23⟩) are visible, while BSFs are out of contrast. The blue square marks a region randomly selected to evaluate the dislocation density. The dislocation densities measured from
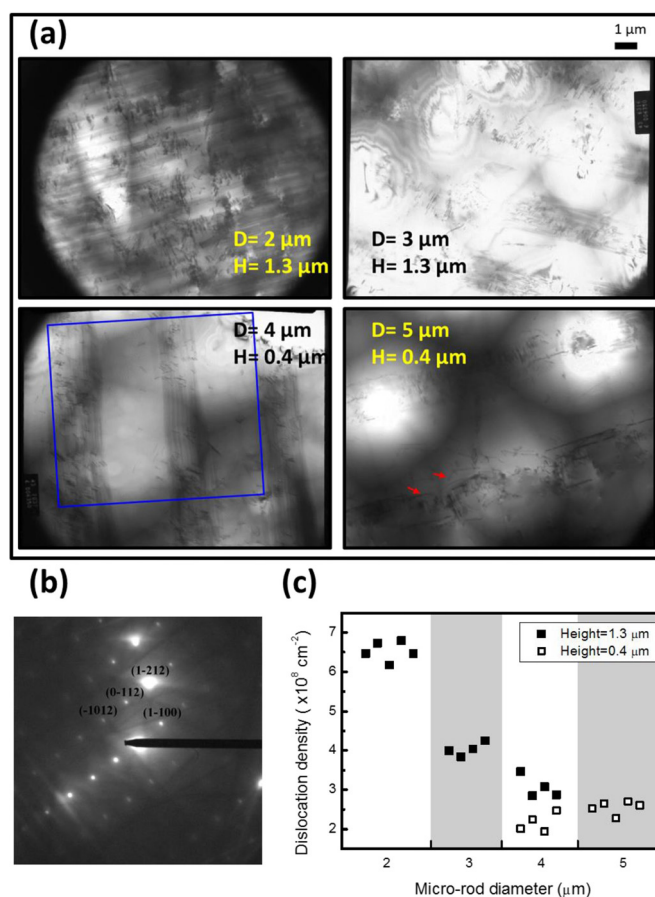

FIG. 3. (a) Bright field plan-view TEM images of semi-polar (11-22) GaN films overgrown on the micro-rods with different diameters and heights, presenting the dislocation distributions across the surface, where the specimens are viewed along the [22-43] zone-axis with the diffraction vector *g* = 1-212 and the diffraction pattern is shown in (b); (c) Dislocation density of the overgrown (11-22) GaN plotted against the micro-rod diameter. Filled and open symbols represent the micro-rods with different heights of 1.3 and 0.4 μm, respectively.

the TEM observation are plotted against the micro-rod diameter in Figure 3(c). The dislocation density shows a reduction from 6.5 × 10^8 cm^{-2} in the case of using a 2 μm micro-rod diameter down to 2.0 × 10^8 cm^{-2} in the case of using a 4 μm micro-rod diameter. Unexpectedly, the dislocation density increases slightly when the micro-rod diameter is further increased to 5 μm with other conditions remaining unchanged. This is different from the BSF behaviors. In addition, threading dislocations with a long dislocation line (marked by red arrows) have been observed in the case of using a 5 μm micro-rod diameter. They are likely generated due to the extended coalescence process as a result of using the micro-rods with a larger diameter.

Furthermore, the crystalline quality of the samples has been characterized by performing X-ray diffraction measurements in order to make a comparison with the above TEM data. Generally speaking, the crystal quality of (11-22) GaN can be evaluated by measuring the full width at half maximum (FWHM) of on-axis X-ray rocking curves as a function of an azimuth angle (labeled as Ψ). Typically, the FWHM at the 0° azimuth angle shows the largest value and the FWHM at the 90° azimuth angle the lowest value,[16–18] and these two FWHMs can be used to represent the crystal quality of
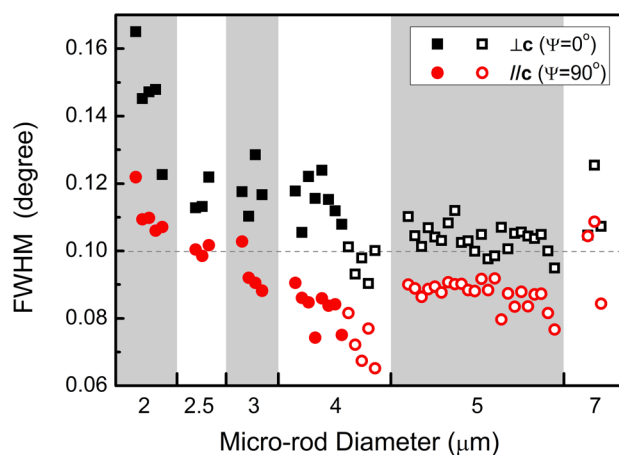
FIG. 4. A summary of the FWHMs of the on-axis XRD rocking curves of the overgrown (11-22) GaN as a function of the micro-rod diameter. Filled and open symbols represent the micro-rods with different heights of 1.3 and 0.4 μm, respectively.

(11-22) GaN. The azimuth angle is defined as zero when the projection of the incident X-ray beam is parallel to the c-direction of (11-22) GaN. Figure 4 provides a summary of the two FWHMs from a large number of the overgrown samples as a function of the micro-rod diameter from 2 to 7 μm. For the as-grown semi-polar GaN templates used for the fabrication of micro-rod templates, the FWHMs are 1345 arc sec (0.374°) and 625 arc sec (0.174°) at the 0° and 90° azimuth angles, respectively. All the overgrown semi-polar GaN films show a significant reduction in FWHM compared with the as-grown templates. With increasing the micro-rod diameter, the FWHMs at both the 0° and the 90° azimuth angles decrease and reach the lowest values in the case of using a 4 μm micro-rod diameter, demonstrating the FWHMs of 325 and 235 arc sec at the 0° and the 90° azimuth angles, respectively. However, with further increasing the micro-rod diameter to 5 and 7 μm, the FWHMs at both the 0° and the 90° azimuth angles increase slightly, meaning an increase in dislocation density. The slight degradation of the crystal quality in the case of using the larger micro-rod diameters agrees well with the dislocation densities measured by TEM as shown in Figure 3(d). Both the XRD data and the TEM data represent a record crystal quality of (11-22) GaN obtained on sapphire substrates. Overall, these low FWHM values are comparable to those for commercial *c*-plane GaN LEDs, implying a great potential to achieve outstanding optical devices on these semi-polar (11-22) GaN films. Furthermore, our previous report based on the micro-rod templates with a small micro-rod diameter showed a 346 arc sec FWHM of XRD rocking curve,[19] while the present study provides XRD data as a function of micro-rod diameter including a record narrow FWHM of XRD rocking curve which is 235 arc sec (achieved using a 4 μm micro-rod diameter). This further confirms a step-change in crystal quality. It is worth highlighting that stimulated emission has been achieved on our semi-polar (11-22) GaN overgrown on the micro-rods with a 4 μm diameter and

a 0.4 μm height, despite the fact that the BSF density in the 4 μm sample is not the lowest (while the 4 μm sample shows the lowest dislocation density). This suggests that dislocations instead of BSFs may play a critical role in determining the optical performance of (11-22) semi-polar GaN based emitters.

In conclusion, semi-polar (11-22) GaN films overgrown on micro-rod arrays with different diameters have been investigated. The PL intensity ratio of the NBE emission to the BSF related emission exhibits a monotonic increase with increasing the micro-rod diameter. TEM measurements further demonstrate that the lower BSF density can be obtained in the (11-22) GaN overgrown on larger and shorter micro-rods. On the other hand, the dislocation density in the GaN films decreases to the lowest value with increasing the micro-rod diameter of up to 4 μm. The XRD measurements confirms that the best crystal quality of the overgrown (11-22) GaN is achieved by overgrowth on micro-rods with a 4 μm diameter and a 0.4 μm height, leading to achieving stimulated emission.

[1]T. Wang, Semicond. Sci. Technol. **31**, 093003 (2016).
[2]A. E. Romanov, T. J. Baker, S. Nakamura, and J. S. Speck, J. Appl. Phys. **100**, 023522 (2006).
[3]T. Takeuchi, S. Sota, M. Katsuragawa, M. Komori, H. Takeuchi, H. Amano, and I. Akasaki, Jpn. J. Appl. Phys. **36**, L382 (1997).
[4]F. Scholz, Semicond. Sci. Technol. **27**, 024002 (2012).
[5]J. E. Northrup, Appl. Phys. Lett. **95**, 133107 (2009).
[6]X. Ni, U. Oüzgüür, A. A. Baski, H. Morkoç, L. Zhou, D. J. Smith, and C. A. Tran, Appl. Phys. Lett. **90**, 182109 (2007).
[7]J. Bai, B. Xu, F. G. Guzman, K. Xing, Y. Gong, Y. Hou, and T. Wang, Appl. Phys. Lett. **107**, 261103 (2015).
[8]H. Asamizu, M. Saito, K. Fujito, J. S. Speck, S. P. DenBaars, and S. Nakamura, Appl. Phys. Express **1**, 091102 (2008).
[9]Y. Enya, Y. Yoshizumi, T. Kyono, K. Akita, M. Ueno, M. Adachi, T. Sumitomo, S. Tokuyama, T. Ikegami, K. Katayama, and T. Nakamura, Appl. Phys. Express **2**, 082101 (2009).
[10]B. Xu, Y. Gong, K. Xing, L. Jiu, Y. Zhang, L. C. Wang, J. Bai, and T. Wang, "Stimulated Emission From Semipolar (11-22) GaN Overgrown On Sapphire," Appl. Phys. Lett. (submitted).
[11]T. Wang, K. B. Lee, J. Bai, P. J. Parbrook, R. J. Airey, Q. Wang, G. Hill, F. Ranalli, and A. G. Cullis, Appl. Phys. Lett. **89**, 081126 (2006).
[12]Y. Zhang, J. Bai, Y. Hou, R. M. Smith, X. Yu, Y. Gong, and T. Wang, AIP Adv. **6**, 025201 (2016).
[13]R. Liu, A. Bell, F. A. Ponce, C. Q. Chen, J. W. Yang, and M. A. Khan, Appl. Phys. Lett. **86**, 021908 (2005).
[14]P. De Mierry, N. Kriouche, M. Nemoz, and G. Nataf, Appl. Phys. Lett. **94**, 191903 (2009).
[15]F. Wu, Y.-D. Lin, A. Chakraborty, H. Ohta, S. P. DenBaars, S. Nakamura, and J. S. Speck, Appl. Phys. Lett. **96**, 231912 (2010).
[16]Q. Sun, B. Leung, C. D. Yerino, Y. Zhang, and J. Han, Appl. Phys. Lett. **95**, 231904 (2009).
[17]M. A. Moram, C. F. Johnston, J. L. Hollander, M. J. Kappers, and C. J. Humphreys, J. Appl. Phys. **105**, 113501 (2009).
[18]M. B. McLaurin, A. Hirai, E. Young, F. Wu, and J. S. Speck, Jpn. J. Appl. Phys. **47**, 5429 (2008).
[19]Y. Gong, K. Xing, B. Xu, X. Yu, Z. Li, J. Bai, and T. Wang, ECS Trans. **66**, 151 (2015).